Crystallisation from Anisotropic Polymer Melts

Daniel P. da Silva[1], James J Holt[2], Supatra Pratumshat[3] Paula Pascoal-Faria[1], Artur Mateus[1],

and Geoffrey Robert Mitchell[1]*

[1] Centre for Rapid and Sustainable Product Development, Polytechnic of Leiria, Marinha Grande, Portugal

[2]Department of Physics, University of Reading, Whiteknights, Reading UK

[3] Department of Chemistry, Faculty of Science, Naresuan University, Phitsanulok, Thailand

*geoffrey.mitchell@ipleiria.pt

Abstract

In situations where the stereoregularity of the polymer chains permits, crystals can form in synthetic or natural polymers. These crystals have an immnse impact on the properties of the polymeric material. Typically polymers crystallised from a quiescent melt form spherulites but where the melt exhibits a level of anisotropy, the crystalline morphology which develops is quite different to the spherulitic structure, although it may well contain chain folded lamellar crystals. We consider a number of different systems in which the anisotropy has developed in different ways. Despite these differences there are strong features in common within the semi-crystalline polymer morphology. We consider the strain-induced crystallization in deformed natural rubber, in sheared melts, in shear melts containing both self-assembling nanoparticles and engineered nanoparticles and during extrusion as part of fused granular deposition based 3D printing.

1.Introduction

The inherent chemical connectivity of polymer molecules develops a local anisotropy and a general challenge in polymer science is how to transform this local anisotropy to the global scale so that it can influence and transform the properties of objects fabricated from that polymer. The natural configuration of polymer chains in the molten state is a random coil [1] and developing a material with extended chains over the full length of the molecule requires very specific processing. In some cases semi-rigid molecules which exhibit a liquid crystal phase over a limited temperature can be processed in to materials with a high level of preferred orientation of the chain axes as a consequence of the long-range orientational order exhibited by such materials [2]. In order to reduce the processing temperatures of such materials, these are typically random copolymers of a variety of aromatic esters. Despite the random nature of the crystals, it has been shown that a small level of crystallinity develops through the formation of nonperiodic crystals [3]. This chapter is focused on the formation of crystals in anisotropic polymer melts, in which the crystals are generally but not exclusively chain folded lamellar crystals. We show that the templating of crystals using anisotropy present in the polymer melt is a powerful control process for defining the morphology and properties of polymer products. We explore various material systems and polymer processing technologies to emphasis the generality of the templating process. We start with the deformation of a network to induce a critical level of anisotropy and then explore the properties of polymer melts using shear flow to impart anisotropy. We extend the concept of anisotropy to include self-assembled nanoscale networks and to engineered nanoparticles such as nanotubes. We conclude by applying this approach to the emerging field of 3D printing and develop the concept of morphology mapping as an extension to 3D printing.

2. Evaluating Anisotropy

In this work we will evaluate the level of preferred anisotropy present in the melt phase and how this is translated to the preferred orientation present in the semi-crystalline morphology. There are many techniques which can be employed to quantitatively evaluate the level of preferred orientation in a polymeric material. Key to a useful analysis is the identification of the structural unit on which the measurements are based, the identification of the axes which are used to define the preferred orientation

and the scale over which the evaluation is made [4]. Polymers provide rich hierarchical structures from bonds to chains to crystals, and it is critical that we are able to define what is being measured. We have found that x-ray and neutron scattering techniques provide a powerful framework for the evaluation of preferred orientation over a range of length scales [5], and in this chapter we will focus on their use. It is also possible to use such techniques for in-situ measurements, the nature of the time-resolution varying between x-ray and neutron scattering. X-ray and Neutron scattering are rigorous techniques [6,7,8] which can be performed in a quantitative manner. We will now present an overview of a framework for evaluating the level of preferred anisotropy from scattering patterns, further details are available in the literature cited. The common symmetry of deformed samples in a polymer context, is a uniaxial symmetry and so we follow this approach here.

The scattering for a sample exhibiting a partial level of preferred orientation can be written as the convolution of the scattering for a perfectly aligned system $I^0(|\underline{Q}|, \alpha)$ with the orientation distribution function $D(\alpha)$ [9,10] :

$$I\left(|\underline{Q}|,\alpha\right) = I^0\left(|\underline{Q}|,\alpha\right) * D(\alpha) \qquad \text{Equation 1}$$

The function $D(\alpha)$ describes the distribution of the structural units with respect to the symmetry axis of the sample.

If we write the intensity functions and the orientation distribution function in terms of a series of spherical harmonics, $I_{2n}(|\underline{Q}|)$, $I^0_{2n}(|\underline{Q}|)$ and D_{2n} we can write this convolution as [Mitchell 2005]:

$$I_{2n}(|\underline{Q}|) = \left\{\frac{2\pi}{(4n+1)}\right\} D_{2n} I^0_{2n}(|\underline{Q}|,\alpha) \qquad \text{Equation 2}$$

where n=0,1,2,3…∞. Only the even terms of each series are required due to the inversion centre intrinsic to a x-ray scattering pattern for a weakly absorbing sample.

The components of each series can be obtained by:

$$I_{2n}(|\underline{Q}|) = (4n+1)\int_0^{\pi/2} I\ (|\underline{Q}|,\alpha) P_{2n}(\cos\alpha)\sin\alpha.d\alpha \qquad \text{Equation 3}$$

and related expressions. The complete scattering pattern and equivalent functions may be recovered by:

$$I(|\underline{Q}|,\alpha) = \sum_{2n=0}^{2n=\infty} I_{2n}(|\underline{Q}|)P_{2n}(\cos\alpha) \qquad \text{Equation 4}$$

We can see that one of the advantages of using scattering techniques is that we can address all components of the orientation distribution function, whereas, the measurement of birefringence or absorption only yield values for $\langle P_2 \rangle$. Here we use angular brackets to indicated an average over the volume of the sample evaluated through the area of the beam and the thickness of the sample. Figure 1 shows a plot of the first four Legendre Polynomials in polar coordinates.

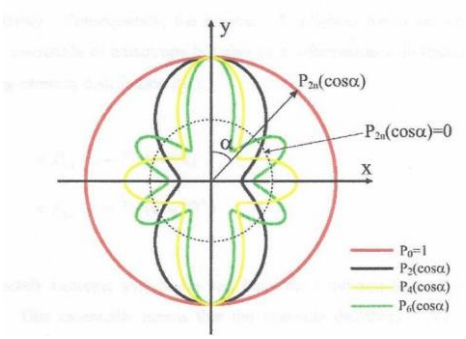

Figure 1 Plots in polar coordinates of the values of the first four Legendre Polynomials

In Figure 2 we show the intensity recorded for a sample of isotactic polypropylene at a particular value of Q plotted in polar coordinates and we can see more clearly the process involved here. Essentially we are identifying the fraction of the shape of the intensity in polar coordinates of each particular function shown in Figure 1 and then scaling that with the scattering for a perfectly aligned system. Key to the usefulness of this approach is the orthogonal nature of the Legendre Polynomials. The process is similar to the use of Fourier Components to describe peak shapes and the convolution is the equivalent the Stokes Theorem.

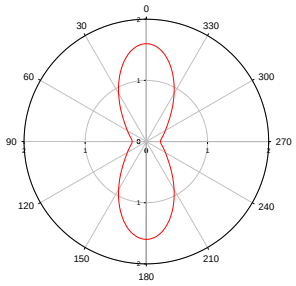

Figure 2 A polar plot of the intensity of the SAXS intensity for a sample of isotactic polypropylene crystallised from a sheared melt at a particular value of Q

It is more convenient to work with normalized harmonics rather than the unnormalized versions inherent in equation 3. The normalized versions of the global orientation parameters $<P_{2n}>$ can be obtained using the equation [11,10]

$$< P_{2n}^{a} \cos(\alpha) >= \frac{I_{2n}^{a}(|\underline{Q}|)}{I_{0}^{a}(|\underline{Q}|)(4n+1)P_{2n}^{m}(\cos\alpha)} \qquad \text{Equation 5}$$

These parameters have values which lie between -0.5 and 1 with a value of 0.0 representing an isotropic arrangement. A value of 1 corresponds to a situation where all structural elements are aligned with a common axis. A value of -0.5 corresponds to a situation where the structural units are aligned orthogonal to the common axis. In some literature $<P_2>$ is referred to as the Hermans Orientation Function, but these are essentially equivalent.

One final comment about this approach is that we will need to ensure that the scattering which is used to evaluate the preferred orientation only includes the scattering from the identified structure, such as crystals. This is usually easily achieved by examination of the Q dependence. This framework provides many advantages which include the identification of multiple components in mixtures [10] and the deconvolution of orientation measured in poorly aligned fibres [12].

3. Crystallisation during deformation of networks

Research on strain-induced crystallization in natural rubber is as old as polymer science itself [13]. The very first reference to crystallinity in strained natural rubber, involved the recently developed technique of X-ray diffraction and was due to Katz [14] and the work played a part in convincing skeptical scientists to accept Staudingers concept of long chain molecules. Katz showed that the crystals which form have a high preferential alignment. Since that early start, numerous researchers have revisited the topic bring new methods and quantitative analysis techniques. Amongst early pioneers in this area was the work of Mitchell [14], who used quantitative static testing to establish the key features. In that work, the scattering associated with the crystals was separated from the amorphous scattering and used to estimate the level of crystallinity. The azimuthual variation of the amorphous interchain scattering was used to evaluate the level of preferred orientation present in the amorphous material. The experimental data exhibited an almost linear variation with strain until λ=4.5 after which it exhibited a sharp upturn eventually reaching a value for $\langle P_2 \rangle$ of ~0.08 at λ=7. The lateral width of the almost perfectly aligned crystals was estimated to be 50Å.

Figure 3 shows data from a recent study using the NCD-SWEET SAXS/WAXS beamline at the ALBA Synchrotron Light Source in Barcelona to record data during the uniaxial deformation of natural rubber [16]. Here we superimposed WAXS patterns taken at specific strains during the loading and unloading parts of the cycle. The well defined arced spots can be seen once the extension ratio λ exceeds 4.2. Upon unloading, the crystalline spots decrease in intensity and eventually disappear when λ< 4.0. In these experiments SAXS patterns were recorded and exhibit an increasing level of anisotropy and an example is shown in Figure 4. This scattering was located around the zero angle point and was typical of isolated anisotropic systems. The scattering did not show any of the characteristics of stacks of chain folded lamellar crystals. The key feature we can note from this work is the near perfect orientation of the crystals. When the network is deformed, some shorter strands become fully aligned before the remaining chains and these chains nucleate the crystals. Small-angle X-Ray scattering data were obtained undertaken as part of the same series of experiments on natural rubber, shows only evidence of isolated crystals and there is no evidence for stacks of crystals as typically forms in a strained uncross-linked melt. Figure 4 shows one of the SAXS patterns corresponding to Image 1c in Figure 3.

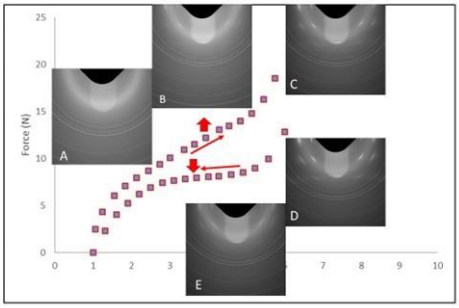

Figure 3 A summary of a uniaxial deformation experiment with WAXS patterns recorded at specific strain points during the loading and unloading superimposed on the plot for the force-strain curve. WAXS patterns were recorded at A) λ=1.0, B) λ=4.3, C) λ=5.75, D)λ=6.0, E)λ= 4.61. The vertical red up arrow marks the strain at which crystalline spots were first observed and the vertical red down arrow marks the strain at which all crystalline spots were no longer observed on unloading when λ< 4.0. The WAXS patterns also show some crystalline diffraction rings which are associated with compounds added to enable cross-linking.

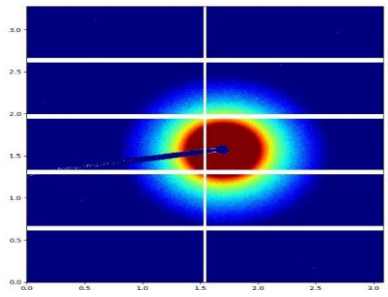

Figure 4 SAXS pattern for a sample deformed with l ??

The study of strain-induced crystallization in natural rubber is complicated by the possibility of thermal crystallization of the rubber. Kohjiya (17) has proposed that strain-induced crystallization should be renamed as "Template Crystallisation" to emphasise the unique characteristics of the process. The process occurs readily in

natural rubber due to the very high stereoregularity of the polymer chains at 99.98%, a characteristic which yet to be exhibited by synthetic *cis* 1,4-polyisoprene. The contribution of X-Ray diffraction to the study of strain-induced crystallisation of natural rubber has been comprehensively reviewed by Huneau [18] and it deals with the effects of strain rate variation and the influence of temperature on the overall process. Sotta et al [19] has revisted Flory's theory of strain induced crystallisation of rubber using recently obtained data and they conclude this provides a good description of the process which is driven by the relaxation of the "amorphous" part of an extended network chain. There is now a comprehensive set of new data and an excellent opportunity to move forward with this topic. Numerous authors emphasise the enhanced sensitivity of theory to measurements made under biaxial deformation and we have already made a start in this direction [20].

4. Sheared Polymer Melts

The rheology of the typical polydisperse polymer melt used to fabricate plastic parts remains a challenging area, but excellent progress has been made with quantitative analysis [21]. However, the basic concepts have been established for some time. In the flow conditions present during manufacturing the longest chains become extended, allowing the majority of the chains to be a relaxed state. As the molten material cools, if the crystallization point is reached with the long chains still extended, then these serve as row nuclei and template the crystallisation so that the chain folded lamellar crystals grow out normal to the row nuclei. The row nuclei all have a common axis of alignment and as a consequence, the initial crystals are almost perfected aligned. Clearly it would be most helpful to observe these very early stages of nucleation using SAXS/WAXS measurements. Pan et al [22] have claimed to observe the SAXS of the so-called shish nuclei. These are very challenging experiments as the contrast between the nuclei and the melt is very low. We have adopted a different approach in which we make use of small-angle neutron scattering of deuterium labelled mixtures of polyethylene, using a parallel plate shear cell to impose some anisotropy on the melt [23].

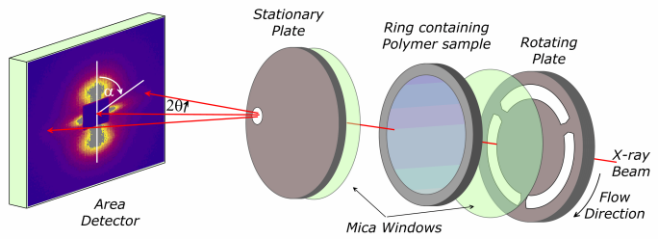

Figure 5 A schematic of the shear cell used for in-situ x-ray and neutron scattering studies

Figure 5 show a schematic of the parallel plate shear cell which was previously used for SAXS/WAXS measurements using thin mica sheets as windows [23]. One of the advantages of designing sample stages for SAXS/WAXS measurements is that the beam size is relatively small < 0.5mm, in contrast the weaker interaction of neutrons with matter results in a larger beam to increase the signal size. For this work we utilized the LOQ spectrometer at the UK Pulsed Neutron Facility ISIS [24] and we used a beam size of 3mm. To accommodate this beam size, we modified the original design of the shear cell and widened the windows and replaced the lead rotating mask with one fabricated from cadmium to reduced any background scattering as the spokes passed through the incident beam. We continued to use mica as the window material. To link to existing SAXS/WAXS experiments [25] we used a commercial PE resin which exhibited a polydisperse molecular weight with a high molecular weight fraction and formed shish-kebab or row nucleated structures [26].

Figure 6. the shear cell on the LOQ Instrument at ISIS in the UK. The incident neutron beam enters from the right, the window to the detector is visible on the right.

To provide contrast we mixed this PE with a deuterated branched PE formed by deuterating a copolymer of polybutadiene. Table 1 shows the characteristics of the materials used in this work. We prepared two mixtures, the first for the SANS experiments were a 10% of A and 90% B, and for the WAXS 10% of A and 90% of C.

In Figure 7, we compare the SANS patterns recorded for this mixture in the quiescent state and subject to shear. There are differences, but it is evident that the SANS pattern recorded during shear flow does not exhibit a highly anisotropic state. To analyse the complete pattern we calculate a series of spherical harmonics which collectively represent the pattern but which serve to separate the orientational behaviour from the structural dependent components (Equation 3).

Table 1 Characteristics of Sample used for SANS Experiments

	PE Sample	F	10^5 Mw	Mw/Mn	SCB	Catalyst
A	HPE	0.10	3.45	9.6	None	Zg
B	DPE	0.90	1.80	1.06	< 1.7% C2	-
C	BPE	0.10	1.60	1.03	< 1.2% C2	-

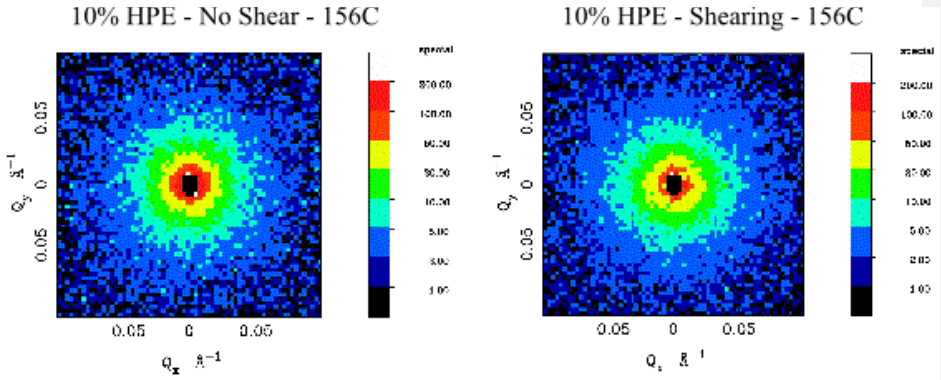

Figure 7 SANS Patterns

Taking the approach described in Section 2 for the pattern shown in Figure 7b yields the plot shown in Figure 8.

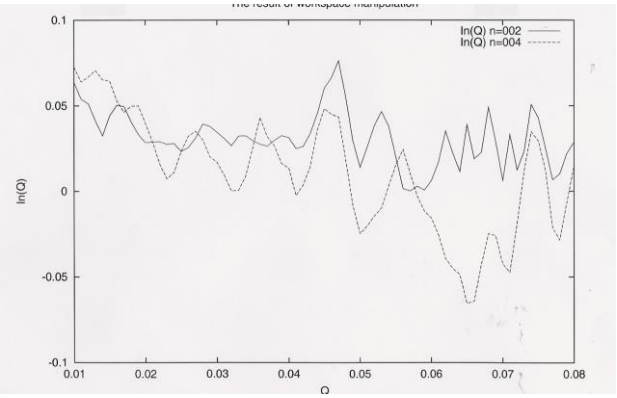

Figure 8 Plots of the Harmonics $I_2(Q)$ and $I_4(Q)$ for the sheared sample (Figure 7b)

And although the data is a little noisy due to the low level of anisotropy we can observe that the Harmonics $I_2(Q)$ and $I_4(Q)$ a more or less constant value which is independent of Q. This contrasts with the calculated harmonics of the scattering for an anisotropic gaussian chain shown in Figure 9 with Rg parallel of 110Å and Rg Perpendicular of 100Å.

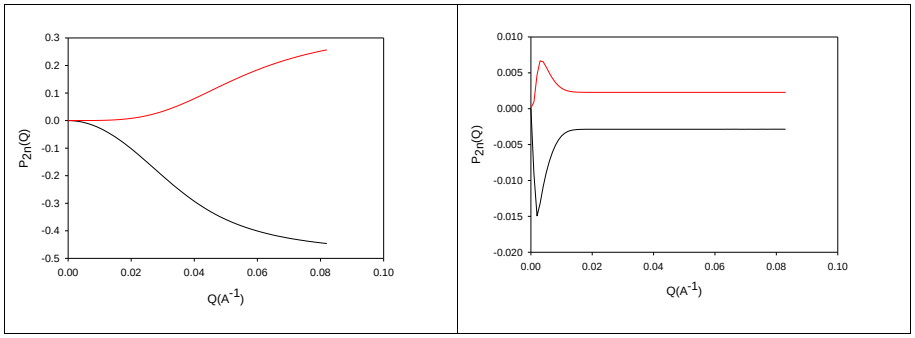

Figure 9 Plots of the calculated first two harmonics I_2 and I_4 for (left) a model of anisotropic Gaussian Chains with Rgparallel = 110Å and Rgperpendicular = 100Å and (right) a model containing 90% of isotropic Gaussian chains with Rg=100Å with 10% of anisotropic Gaussiaan chains with an anisotropy ratio of 10 in the radius of gyration.

The strong Q dependence of these calculated harmonics (Figure 9 left) contrasts strongly with the observed harmonics.

A possible alternative model takes isotropic gaussian chains with Rg of 100Å together with a small fraction of highly anisotropic gaussian chains, the latter with a ratio of Rg parallel/Rg perpendicular of 10 and the calculated harmonics are shown in Figure 9 (right)

This reproduces the essential features of the experimental harmonic functions in exhibiting a constant level of the harmonic as a function of Q. Of course if we were able to record data at very low Q values then there would be a rise in the values and the development of a Q dependence, but that scattering region is not experimentally accessible on LOQ. The value of the constant value of the harmonics is directly related to the fraction of anisotropic gaussian chains as Figure 10 shows.

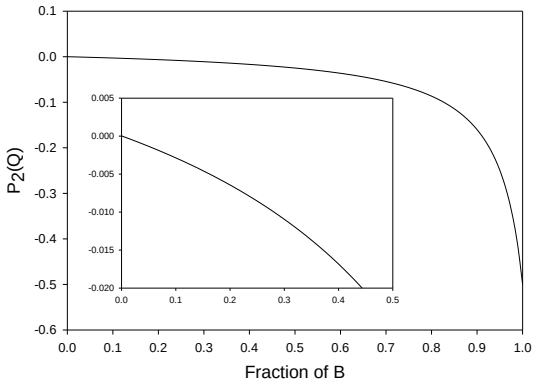

Figure 10 A plot of the value of the harmonic $\langle P_2 \rangle$ as a function of the Fraction of highly anisotropic chains

This suggests the molten polymer contains a small fraction of highly extended chains within a matrix of isotropic chains. This result is supported by orientation measurements made using WAXS [26].

We have explored the consequence of shear flow on the crystallization behaviour of an equivalent undeuterated system. We have prepared mixture of the BPE and the high molecular weight linear HPE (A+C) as shown in Table 1. In order to fully appreciate the behavior of the mixture, we need to examine the properties of the

components.

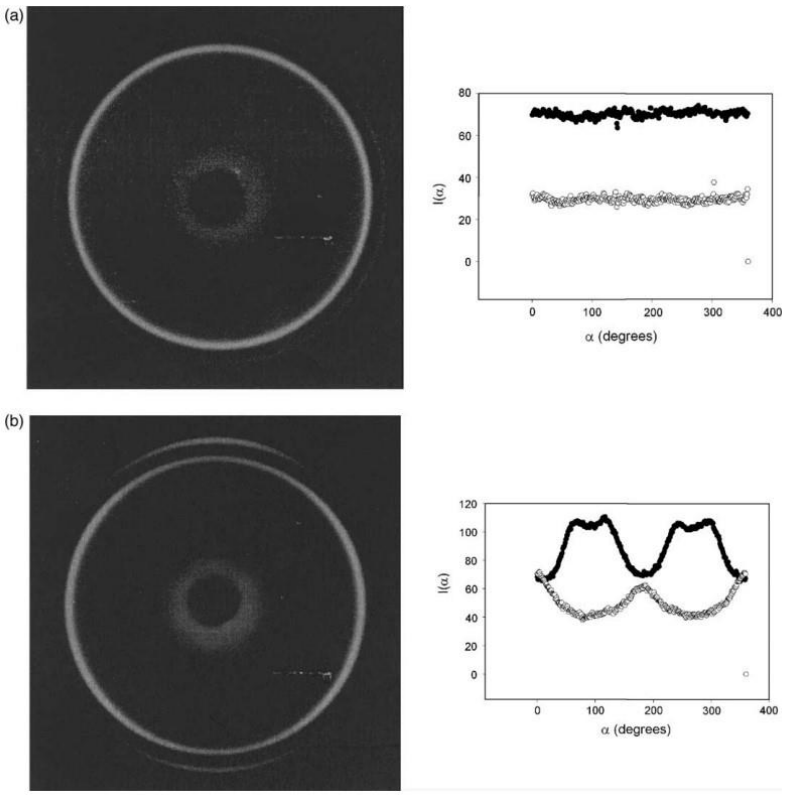

Figure 11 WAXS Patterns of a mixture of PE sheared as in Figure 7 and cooled rapidly to room temperature. The plots show the aziimuthual sections for the 110 and 200 peaks

Figure 11 shows WAXS patterns for samples of BPE(a) and HPE(b) sheared at 150°C at a shear rate of $10s^{-1}$ for shear strain of 100 shear units and then the shear was halted and the sample cooled quickly to room temperature. The right-hand curves are azimuthual sections at the peak positions of the (110) and the (200) reflections. As can be seen from the patterns, the BPE exhibits no anisotropy in the crystal peaks and similar results were obtained for shear rates up to $30s^{-1}$ [25]. In contrast the HPE showed a significant level of preferred orientation, in which the azimuthual position of the maximum in the crystal reflections was dependent on the shear rate [26].

Figure 12 is a transmission electron micrograph of a differentially etched internal surface of the sample used for Figure 11. It exhibits a very high level of preferred orientation. There are features running from top to bottom which reflect the

row nuclei or shish which have directed or templated the remaining structure. We can also observe the chain folded lamellar crystals, largely edge on running across the micrograph. This underlines the massive amplification that takes place with respect to the level of preferred orientation upon crystallization from a deformed melt. It is noteworthy to emphasise that in this mixture there is a high molecular weight fraction which is very responsive to the applied shear flow and the BPE whose crystallization is not influenced by the shear flow. What we find here is that all these molecular species have been templated in to a high level of preferred orientation.

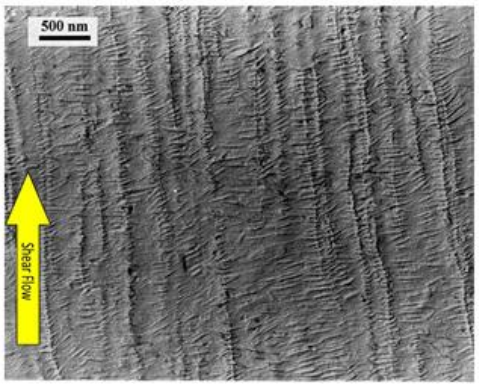

Figure 12 A TEM micrograph of a replica of a differentially etched internal surface of the sample (Figure 9)

5. Crystallisation during injection moulding

Injection moulding is the most widely used technology for the fabrication of plastic parts. In this technique, molten plastic is injected at high pressure in to a metal mould with a cavity which replicates the shape of the desired product. The mould is maintained at a much lower temperature then the molten plastic so that the plastic solidifies through a glass transition or through crystalllisation in the case of a crystallizable polymer. In fact semi-crystalline polymers in the form of isotactic polypropylene and polyethylene are amongst the most widely used materials. Injection moulding has evolved in to a high technology process and now moulds are digitally designed and the injection moulding process is fully tested and explored in the virtual sense within simulations. The structure and morphology of injection moulded products has been widely studied [28,29]. This shows that the morphology develops in stages and it would be very useful to be able to follow these developments in real-

time. The flow rates and the cooling/heating rates are considerable and are greatly different to those available with the shear cell used in the previous section. Recently two groups have taken on the challenge of developing experimental techniques which allow the structure and morphology to be evaluated in real-time using x-ray scattering techniques. These two groups have followed different pathways, one involving the current authors have developed an industrially relevant injection moulding system which can be mounted on the NCD-SWEET ALBA Sychrotron Light Source [30,31]. Figure 13 shows a schematic of the equipment which is based on traditional metal mould design procedures.

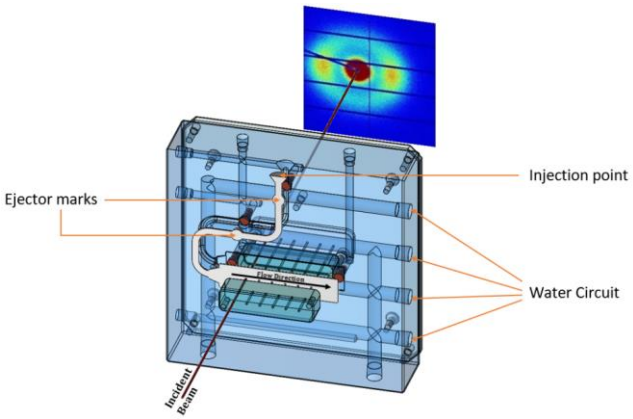

Figure 13 A schematic of the industrially relevant injection moulding system developed by Mitchell and co-workers, reproduced from [31].

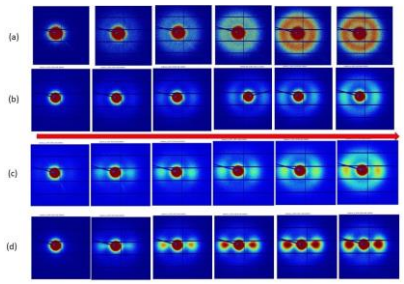

Figure 14 SAXS patterns for isotactic polypropylene immediately after injection in the mould. Time moves from left to right on a 1s time interval. The four sequences correspond to injection temperatures of (a)250°C, (b) 210°C, (c) 200°C and (d) 190°C reproduced from [31]

Liao et al and Zhao et al have followed a different approach which is focused on micro-injection moulding and uses diamonds as the x-ray transparent windows in the mould

cavity [32,33]. Both of these approaches offer considerable promise for the future understanding and development of crystallization in injection moulding of plastics.

6. Sheared Polymer Melts with Nucleating Agents

In the previous two sections we reviewed results which underline the massive amplification available by templating crystallization using highly aligned chains as row nuclei. The success of this approach encouraged us to explore alternative approaches using nanoparticles embedded in the polymer melt. There is the possibility of adding preformed nano-particles to the melt and these are considered in the next section. In this section we focus on the formation of nanoparticles through self-assembly in the polymer melt, thereby sidestepping the challenges of dispersing the nanoparticles in the polymer melt. There are a number of nucleating agents which are based on small-molecules which self-assemble in to fibrillar extended particles. One of the most widely studied of these is dibenzylidene sorbitol (DBS) [34] (Figure 15) which is widely used as a clarifying agent with polypropylene to stimulate a high density of nuclei to yield a large number of small-crystals with a size smaller than the wavelength of visible light so as to render the final film clear and transparent and suitable for applications typically in packaging [35].

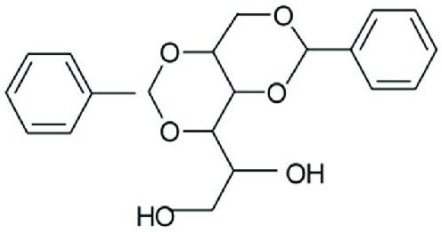

Figure 15 The chemical configuration of dibenzylidene sorbitol

Here we review the work of Nogales et al [36,37] which were based upon a polypropylene copolymer (cPP) with Mw) 2.2×10^5 and Mn) 5.9×10^4 (trade name NOVOLEN 3240NC, BASF plc.), which contains 3.5% ethylene comonomer. They prepared samples of the copolymer with different fraction of dibenzylidene sorbitol in the form of Millad 3905, (Milliken Chemicals) [34]. These were then sheared at 160°C using the equipment shown in Figure 5 at a shear rate of $20s^{-1}$ for a shear strain of 120 shear units. We can see directly that the sample without DBS shows little evidence for an anisotropic structure, but increasing amounts up 5% show increasing levels of preferred orientation

as can be evidenced by the arcing of the x-ray patterns (Figure 16). When 20% of DBS is added there is strong evidence for large scale segregation and a change from the fibrillar morphology.

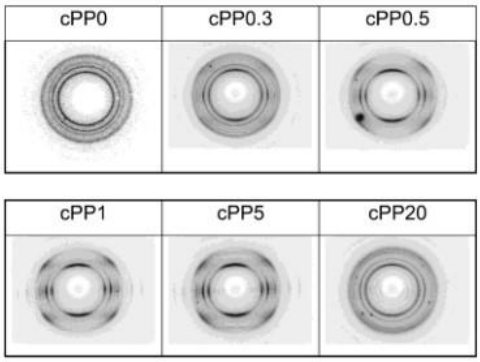

Figure 16 WAXS Patterns of cPP with differing amounts of DBS after shearing before crystallisation

Subsequently Nogales et al also explored the effects of DBS in polyethylene, for which it is widely reported that DBS did not function as a clarifying agent and with poly(ε-caprolactone). Mitchell et al, [38] used SANS to clarify the phase diagram of DBS and PE. They showed that at high temperatures, the DBS was completely soluble in the PE matrix, on cooling, the DBS phase separated through crystallization [38].

They used a linear polyethylene GX 555-2 (from Hoechst, Mn = 24,000, Mw = 171,000 as determined by Rapra Technology, Shawbury Shrewsbury Shropshire United Kingdom SY4 4NR). The polymer is understood to be produced by a metallocene catalyst. The additive, dibenzylidene sorbitol (DBS) (trade name Millad 3905, Milliken Chemicals),[39] was mixed with the polyethylene, 1% in weight, by a solution/precipitation method, involving the initial dissolution of both components in hot xylene, followed by precipitation in an excess of isopentane chilled to near its freezing point with liquid nitrogen. Samples were subjected to shearing in the melt and then cooling to room temperature. These samples with and without DBS were studied on the A2 beamline at the HASYLAB in Hamburg. Figure 17 shows the WAXS patterns.

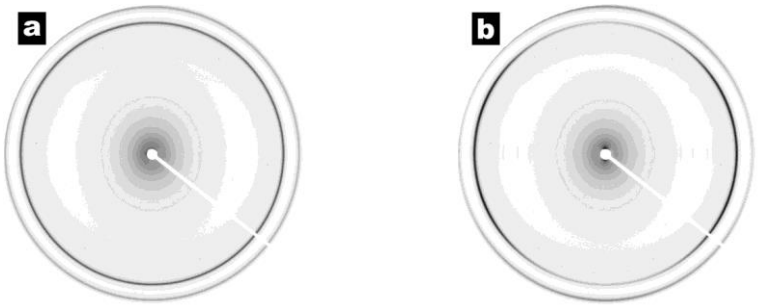

Figure 17 Wide angle X-ray patterns of polyethylene specimens sheared in the melt and subsequently crystallized; (a) without and (b) with added sorbitol based nucleating agent. The flow direction during the shear flow stage is vertical. These distinct crystalline features correspond to the 110 and 200 Bragg reflections. *Note: the outer 200 reflection has been slightly cropped at upper left by the detector, so comparisons should be made of the right and bottom parts of the picture.*

Figure 18 shows a TEM micrograph obtained from a replica of a differential etched internal surface [5] for a sample of polyethylene with 1% of DBS. The micrographs show several troughs which represent where the DBS was before etching. In Figure 18 we can see the actual ends of DBS fibrils, the flat end may be the result of breakage during shear flow. In the area alongside the DBS trough, the polyethylene lamellae run out normal to the DBS fibril surface. In contrast, the lamellae in the region to the left of the ends of the DBS fibrils, the polyethylene lamellae have a different orientation. This clearly demonstrates the templating effect of the DBS fibrils on the lamellae growth.

The influence of the addition of DBS to polypropylene and polyethylene has been extended to polycaprolactone and to the use of some halogenated DBS derivates. The great contrast between between the PCL and the DBS enable Wangsoub et al, [40] to determine that the DBS fibrils were crystalline and that it exhibited a lower solubility in the PCL increasing the number density of fibrils and yield with shear, the highly aligned structure shown

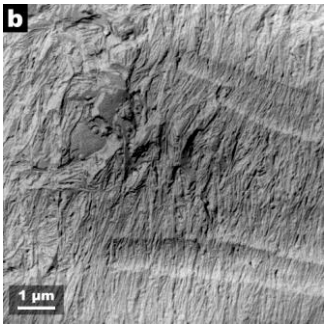

Figure 18 A TEM micrograph of a differentially etched internal surface of a sheared sample of polyethylene with 1%DBS

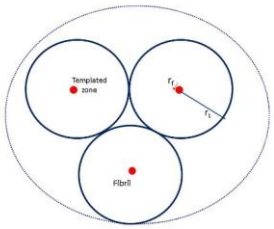

Figure 19 The basic elements of the templating model proposed by Wangsoub et al Reproduced from (Wangsoub et al 2009)

Wangsoub et al [40] developed a quantitative model of templating with DBS Fibrils. In the case of highly aligned fibrils, consideration of the templating process reduces to a 2-d matter. The number density of fibrils is given by

$$N = \frac{(f - f_c)}{\pi r_f^2}$$ equation 6

where f is the fraction of the DBS present in the polymer and f_c is the upper limit of solubility of the DBS derivative in the polymer matrix. We consider all fibrils to have the same radius r_f. Wangsoub et al [41] used SAXS to measure the fibril radius and found that under some conditions, the distribution of fibril radii approach the monodisperse state. If we associate a templated zone of radius r_t with each fibril the fraction of templated material, f_t, is given by:

$$f_t = (f - f_c)\frac{\pi r_t^2}{\pi r_f^2}$$ Equation 7

This is a relatively simple model without any distribution of fibril dimensions and the templated zone size does not account for a random spatial distribution of fibrils. However, we do have an estimate of the fibril radius of ~7.5nm from the SAXS measurements and we have estimated for polyethylene that the templated zone has a radius ~100nm. This suggests that the value of (f – fc) needs to be greater than 0.014 to achieve full templating. Clearly the solubility of the sorbitol derivative in the polymer matrix is critical in determining the actual amount of additive required to achieve this. Wangsoub et al [40] previously estimated that the solubility limit of DBS in PCL was ~0.01. They reported that a chlorine derivative of DBS exhibited a reduced solubility limit in PCL and led to enhanced templating of Cl-DBS. In essence the level of direction was more or less perfect, as can be observed in Figure 20.

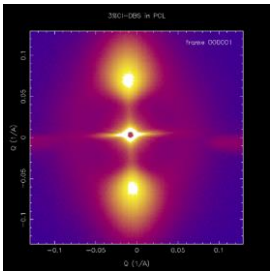

Figure 20 shows the SAXS pattern recorded for the 3% Cl-DBS/PCL system after shearing at 80°C at a shear rate of 10^{-1}s This pattern was ob-tained at the Diamond Light Source beam line I22. Redrawn from Mitchell 2013

The orientation parameter $\langle P_2 \rangle_L$ describing the preferred orientation of the lamellae with respect to the flow axis is given by the fraction of material templated:

$$\langle P_2 \rangle_L = -0.5(f - f_c)\frac{\pi r_t^2}{\pi r_f^2}$$ Equation 8

The factor –0.5 takes account of the fact that the lamellae are arranged normal to the flow axis. Equation 8 shows that efficacy of templating or directing process is directly related to the number density of the DBS fibrils. For a given fraction of DBS, the number density can be optimized by making the nanofibrils as thin as is possible. The processes described in this section are effective as a consequence of the lateral scale of the fibriils. Some have proposed that the interaction between the DBS and

the polymer matrix can be described as atomic level epitaxy. From the universality of the process with differing polymers and differing derivatives of sorbitol, we suggest that this may be more related to topology. We note that Mitchell and Olley [42] have reported the possibility of achieving orthogonal templating by using an additional agent to severely limit the length/breadth of the DBS fibril and this opens up new possibilities which may prove to invaluable for some applications.

7. Sheared Polymer Melts with Nanoparticles

The development of nanocomposites is a major area of activity in polymers. The goal is to fully disperse small fractions of engineered nanoparticles within a polymeric matrix so as to lead to enhanced properties. For a semi-crystalline polymer, the nanoparticles can only be dispersed within the amorphous phase. Carbon nanotubes, Halloysites and other mineral particles as well as graphene nanoflakes have been employed. Avalos-Belmontes et al [43] have reviewed the nucleating behaviour of CNTs in isotactic polypropylene. Mitchell et al [44] have shown that a modest shear rate of $1s^{-1}$ is sufficient to induce a preferred orientation of 14nm graphene nanoplatelets which then templates the crystallization of the PCL matrix. Figure ? shows

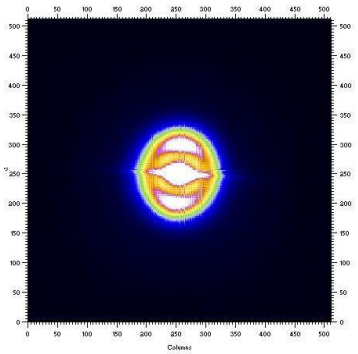

Figure 21 SAXS Pattern recorded for a sample of PCL/graphene sheared for 1000 shear units at 1/s at 100°C and cooled to room temperature. Reproduced from [44]

8. 3D Printing Using Extrusion

3D printing is one of the emerging technologies under the additive manufacturing umbrella which forms part of the 4th Industrial revolution I 4.0 [45]. In this concept, products are manufactured from a digital definition such as a Computer Aided Design file without the use of specialist tooling such as moulds or dies. For that reason it is sometimes referred to as Direct Digital Manufacturing (DDM) which is a more precise description of the process. It involves a variety of technologies such as stereolithography, fused deposition modelling and selective laser melting and addresses both plastics, ceramics and metals. The basic concept of fused deposition modelling in which a preformed thermoplastic filament is fed through rollers into hot extruder and the plastic appears as a molten strand as it emerges from the extruder and is deposited where required on a build platform and the process is repeated layer by layer. Figure 22 (left) shows a schematic of the Fused deposition modelling

.

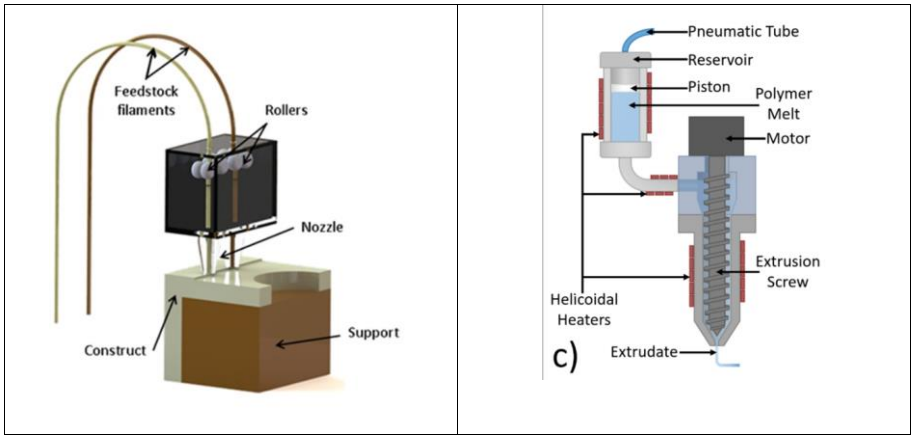

Figure 22 (left)A schematic of the fused deposition modelling 3D printing process (right) a schematic of the fused granular deposition 3D printing, reproduced from [46]

We will now described some work which is focused on 3D printing but using a pellet fed extruder system as shown schematically in Figure 22 (right). This offers several distinct advantages over the filament based methodology. First and foremost it is not necessary to prepare filament of each material, a process which may involve handling a kilogram or more of material. The fused granular printing involves working with small pellets or fragments of

polymers and is hence much more suited to materials development, where the process of producing filaments may be quite severe. Secondly, it allows great control and definition of the extrusion process including both the extrusion die and the extrusion pressure. In some cases we have employed an industrial scale extruder which facilitates the addition of a sensor to provide feedback on the extrusion pressure and enables greater pressures and temperatures to be used.

Of course in the end it is a polymer processing system and all of the lessons learnt in the earlier sections will and must apply. Tojeira and Mitchell [47] were the first to realise that the extrusion process could under certain conditions lead the deposition of material on the build platform which exhibited a high level of preferred orientation of the chain folded lamellar crystals which form on cooling following the printing process [48]. This led on to the development of a 3D printer which could be mounted on the NCD-SWEET ALBA Synchrotron Light Source SAXS /WAXS beamline to evaluate the development of the morphology of the polymer during the 3D printing process and this is described in the following section.

7.1 In-situ Studies of polymer crystallisation during3D printing

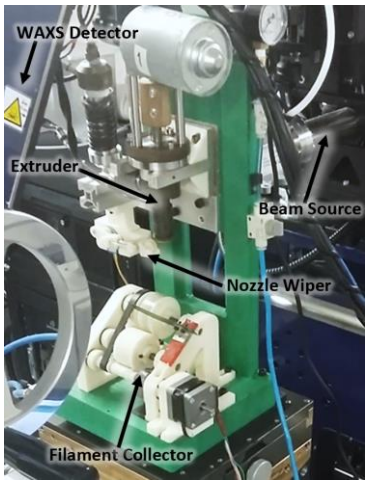

Figure 23 The 3D Fused Granular Deposition Printer mounted on the NCD-SWEET Beam-line at ALBA Synchrotron Light Source Reproduced from [46]].

Figure 23 shows the equipment specifically design for the in-situ 3D printing of thermoplastics on the NCD-SWEET Beamline at the ALBA Synchrotron Light Source in Barcelona, Spain. This

equipment is described in detail elsewhere [46], but in essence it provides the opportunity to follow the progression of development of the semi-crystalline morphology in the extruded filament as it emerges from the extrusion die and cools in a quasi-static manner.

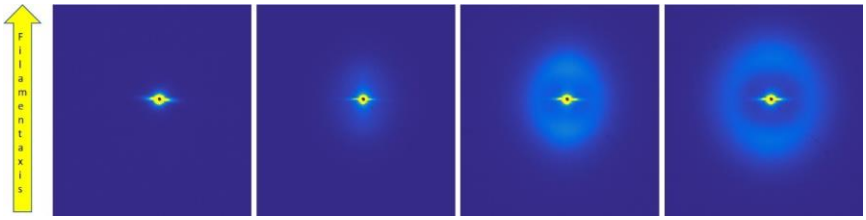

Figure 24 SAXS patterns recorded in-situ from an extruded filament of PCL. The position of the beam is closest to the extruder on the left moving in 0.1mm increments to the left Reproduced from [46]

Now although the extruded filament is moving, the environment is more or less fixed. As a consequence we can move the beam down the extruded filament and this in effect represents the time evolution. In Figure 24 we show a set of SAXS patterns recorded at ALBA using the equipment shown for a sample of PCL extruded at ??C and with a fast write speed. The write speed is the speed of relative displacement of the print head with respect to the build platform. The pattern on the extreme left corresponds to the point closest to the extruder die and the pattern is featureless as the polymer density has no structure or variations in electron density on the scale probed. The next pattern to the right shows weak scattering corresponding to the early stages of crystallization and it appears to be highly anisotropic, but as we move on to successive patterns to the right, a more isotropic structure emerges and becomes the dominant feature. In the final pattern on the right hand size, the scattering is more or less completely isotropic and that initial highly anisotropic scattering is submerged in the mass of isotropic scattering.

Figure 25 shows a second set of patterns obtained using the same procedures as above and with PCL but with a faster write speed, all other conditions being the same. The sequence of patterns is very different to those shown in Figure 24

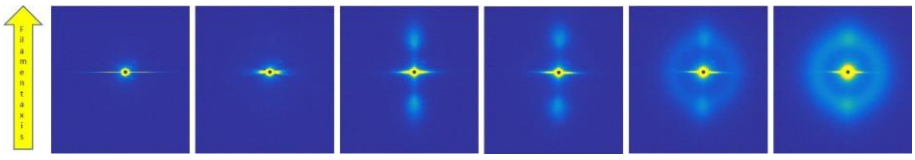

Figure 26 SAXS patterns recorded in-situ from an extruded filament of PCL. The position of the beam is closest to the extruder on the left moving in 0.1mm increments to the left. The print parameters are the same as used in Figure 19, but the write speed is fast. Reproduced from [46]

The sequence starts the same, although the horizontal streak is more extended and probably relates to nanovoids in the extrudate. The next three patterns to the right show a development of a highly anisotropic structure which is typical of a highly aligned stack of chain folded lamellar arranged so that the growth of the lamellar is normal to the extrusion axis. As we have observed in earlier sections this is very typical of row nucleated structures, where nucleation provides a common global axis. The last two patterns to the right show the development of an isotropic crystalline morphology which overlays the initial anisotropic structure. These two different morphologies exhibit different mechanical properties by at least a factor of 2-3x [48]. We can quantify the development of anisotropy in the crystalline morphology using the SAXS patterns as described in section 2 and the results are shown in Figure 28. The advantage of performing time-resolved in-situ measurements can be clearly seen in these plots.

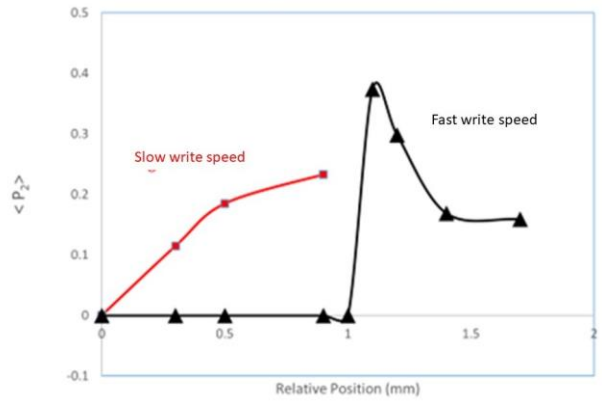

Figure 27 Plots of the global preferred orientation <P2> measured for the SAXS patterns shown in Figures 25 and 26. Reproduced from [46]

Figure 28 (left) shows three SAXS patterns from the 3D printing of LDPE with increasing write speed from left to right. The fastest write speed provides the highest level of preferred

orientation as observed with PCL. Figure 28 (right) show a 3D plot of the global orientational parameter $<P_2>$ as a function of the extrusion speed and write speed for printing LDPE.

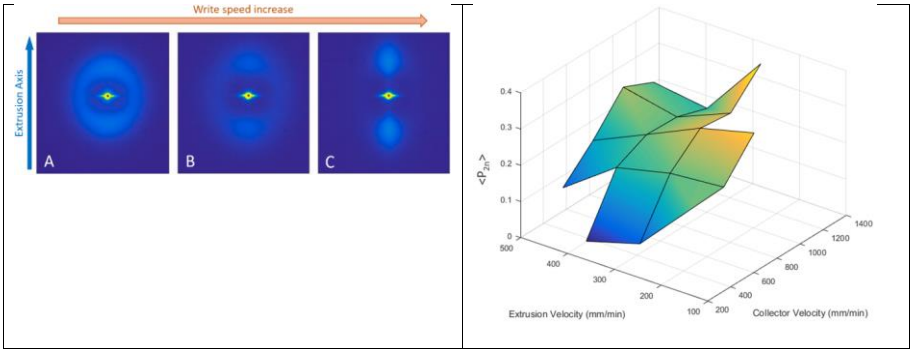

Figure 28 (left) SAXS Patterns measured during 3D printing with an increasing write speed moving left to right. (right) A plot of the global orientation parameter $<P_2>$ for the normals to the chain folded lamellar crystals evaluated using the patterns shown in Figure 29 (left) and related patterns as a function of the extrusion and write speed. Reproduced from [46].

8. Morphology Mapping

Silva et al [46# have introduced the term "Morphology Mapping" to describe the possibility of depositing using fused granular deposition 3D printing, polymeric materials in different parts of the of product with differing properties. The different properties are defined by the print parameters selected at the point of deposition and which can be varied more or less instaneously during printing. This arises directly from the transfer of the directing anisotropy imposed in the melt phase to the semi-crystalline morphology.

9. Discussion

In this chapter we have demonstrated the powerful link between a level of anisotropy in the melt phase and the subsequent morphology of the semi-crystalline state. We observe that crystallization is directed by this anisotropy in the melt to yield a high level of common crystal orientation. Without such direction or templating, the crystals adopt an isotropic morphology. We can clearly see much commonality in these different processes. The process of strain induced crystallization in natural rubber appears to generate the highest level of common crystal orientation. We attribute this to bother the highly extended state of the nucleating chains and that crystallization ocurrs through the templated crystallization of long crystalline chains as chain folding does not take place in the conditions studied. The systems

which contain DBS and derivatives dispersed in the polymer matrix also show very high common alignment for both the chain folded lamellar crystals and the highly acicular nanoparticles that serve as row nuclei. The high aspect ratio (length to breadth ratio) of the nanoparticles will lead to high common alignment with minimum of shear rate and applied shear strain. The high common alignment arises through the directing surface of the DBS nanoparticles and we deduce that through symmetry of that surface the lamellar crystals grow normal to the nanoparticle. Similar considerations apply to the system with graphene nanoplatelets. The generation of row nuclei in a polymer melt is a greater challenge, not least as the random coil configuration has to be unravelled in contrast to the rigid DBS nanoparticles and there are greater opportunities for relaxation again in contrast to the DBS nanoparticles. As a consequence, the resultant highly level of anisotropy present in the semi-crystalline polymer morphology is lower and similar arguments apply to the work on 3D printing. The development of morphology mapping as part of 3D printing of semi-crystalline polymers is an exciting and rapidly growing area.

10. Acknowledgements

This work was supported by the Fundação para a Ciência e Tecnologia (FCT) through the project references: MIT-EXPL/TDI/0044/2021, UID/Multi/04044/2013; PAMI-ROTEIRO/0328/2013 (Nº 022158), Add.Additive—add additive manufacturing to Portuguese industry POCI-01-0247- FEDER-024533 and UC4EP PTDC/CTM-POL/7133/2014).

WE acknowledge the critical role of large scale facilities in this work including the ALBA Synchrotron Light Source in Barcelona, the Daresbury Synchrotron Radiation Source in the UK, the ESRF in France, DESY in Germany, Elettra in Italy and the STFC ISIS Pulsed Neutron Source in the UK and we thank the scientists involved with each beamline for their involvement in this work. The experiments on 3D printing were performed at the NCD-SWEET beamline at ALBA Synchrotron with the collaboration of ALBA staff. We thank EPSRC and BP Chemicals for CASE Award for JJH (University of Reading) and Naresuan University for a PhD scholarship for SP and the Faculty of Science at Naresuan for funding a scientific visit.

11 References

[1] de Gennes P.G. (1979) “Scaling Concepts in Polymer Physics” Cornell University Press Ithaca

[2] Donald, A.M., Windle, A.H., Hanna, S. – 2006, “Liquid Crystalline Polymers” Cambridge University Press, Cambridge UK ISBN 9780521580014

[3]Spontak, R.J. and Windle, A.H. (1992), Crystallite morphology in thermotropic random copolymers: Application of transmission electron microscopy. J. Polym. Sci. B Polym. Phys., 30: 61-69. https://doi.org/10.1002/polb.1992.090300106

[4] Mitchell G.R., Windle A.H. (1988) Orientation in Liquid Crystal Polymers. In: Bassett D.C. (eds) Developments in Crystalline Polymers. Springer, Dordrecht. https://doi.org/10.1007/978-94-009-1341-7_3

[5] Mohan, S.D., Olley R.H., Vaughan, A.S. and Mitchell, G.R. (2016) ‘Evaluating Scales of Structure in Polymers’” in “Controlling the Morphology of Polymers: Multiple Scales of Structure and Processing." Springer ISBN 978-3-319-39320-9

[6] Roe, R-J. 2000 “Methods of X-Ray and Neutron Scattering in Polymer Science” Oxford University Press, Oxford ISBN 0-19-511321-7

[7] Chu B, Hsiao BS (2001) Small-angle X-ray scattering of polymers. Chem Rev 101:1727–1762

[8] Wignall GD, Melnichenko YB (2005) Recent applications of small-angle neutron scattering in strongly interacting soft condensed matter. Rep Prog Phys 68:1761–1810

[9] Deas , H.D., 1952 Acta Cryst 5 542

[10] Mitchell,G.R., Saengsuwan, S.,and Bualek-Limcharoen S., (2005) Evaluation of preferred orientation in multi-component polymer systems using x-ray scattering procedures, Progress in Colloid and Polymer Science 130 149- 159 2005

[11] Lovell, R., and Mitchell, G.R., Acta Cryst (1981) “Molecular orientation distribution derived from an arbitrary reflection”,Acta Crystallographica Section A 37,135-137

[12] Edwards MD, Mitchell GR, Mohan SD, Olley RH (2010) Development of orientation during electrospinning of fibres of poly(ε-caprolactone). Eur Polym J 46:1175–1183

[13] Staudinger, H. (1920) “Über Polymerisation” Ber. Dtsch. Chem. Ges. 1920, 53, 1073–1085. DOI: 10.1002/cber.19200530627

[14] Katz, J.R., (1925) Naturwissenshaften 19 410

[15] Mitchell GR (1984) “A Wide angle X ray Scattering Study of the Development of Molecular Orientation in Cross linked Natural Rubber” Polymer 25 1562-1572

[16] Silva, D.; Pinheiro, J.; Abdulghani, S.; Kamma-Lorger, C.S.; Solano, E.; Martinez, J.C.; Pascoal-Faria, P.; Mateus, A.; Mitchell, G.R. (2022a) Controlling Morphological Development during Additive Manufacturing: A Route to the Mapping of Properties. *Mater. Proc.* **2022**, *8*, 116. https://doi.org/10.3390/materproc2022008116

[17] Kohjiya, S.., (2017) ”Crystallisation of Natural Rubber Its Unique Feature Elastomere und Kunststoffe Elastomers and Plastics 38

[18] Huneau, B., (2011) “Strain-induced Crystallisation of Natural Rubber – A Review of X-ray Diffraction Investigation” Rubber Chemistry and Technology, American Chemical Society 84(3) 425-452 10.5254/1.3601131. hal-01007326

[19] Sotta, Paul, and Albouy, Pierre-Antoine, (2020) “Strain-Induced Crystallization in Natural Rubber: Flory’s Theory Revisited”, Macromolecules, 53, 8, 3097–3109 doi: 10.1021/acs.macromol.0c00515
[20] Lamolinara, B., da Silva, D.P., Gameiro, F., Pascoal-Faria, P., Mateus, A. Martinez, J.C., and Mitchell, G.R., Self-Contained Equipment for the Quantitative Biaxial Deformation of Soft Elastic Materials 2022 Eng submitted
[21] Keller, A. and Kolnaar, H.W.H. (2006) ”Flow-Induced Orientation and Structure Formation. In Materials Science and Tech- 442 nology (eds R.W. Cahn, P. Haasen and E.J. Kramer). **2006**. https://doi.org/10.1002/9783527603978.mst0210
[22] Pan, Y., Li, N., Wang, J., Wang, D., Pan, X., Liu, C., Jian, X., (2021) “The role of expansion angle and speed on shish-kebab formation in expansion pipe extruder head explored by high temperature rapid stretch” Polymer Testing, 104, 107387, doi.org/10.1016/j.polymertesting.2021.107387.
[23] Nogales A, Thornley SA, Mitchell GR (2004) Shear cell for in situ WAXS SAXS and SANS experiments on polymer melts under flow fields J Macromol Sci Physics B 43: 1161-1170.
[24] Heenan, R K; Penfold, J; King, S M. *J. Appl. Crystallogr.* (1997), 30, 1140.
[25] An, Y., Holt, J.J., Mitchell, G.R., and Vaughan, A.S., 2006 Influence of Molecular Composition on the Development of Microstructure from Sheared Polyethylene Melts: Molecular and Lamellar Templating Polymer 47 5643-5656 2006
[26] Pople, J.A., Mitchell, G.R., Chai, C.K. (1996) “In-situ time-resolving wide-angle X-ray scattering study of crystallization from sheared polyethylene melts”, Polymer, 37 4187-4191, doi.org/10.1016/0032-3861(96)00264-9.
[27] Spoerer, Y.; Androsch, R.; Jehnichen, D.; Kuehnert, I. Process Induced Skin-Core Morphology in Injection Molded Polyamide 66. *Polymers* **2020**, *12*, 894. https://doi.org/10.3390/polym12040894
[28] Pantani, R., Coccorullo, I., Speranza, V., Titomanlio, G., (2005) ”Modeling [28of morphology evolution in the injection molding process of thermoplastic polymers” Progress in Polymer Science, 30(12), 1185-1222, doi.org/10.1016/j.progpolymsci.2005.09.001.
[29] Speranza, V.; Liparoti, S.; Pantani, R.; Titomanlio, G. (2019) Hierarchical Structure of iPP During Injection Molding Process with Fast Mold Temperature Evolution. *Materials* **2019**, *12*, 424. https://doi.org/10.3390/ma120304243.
[30] Costa, A.; Gameiro, F.; Potencio, A.; Silva, D.; Carreira, P.; Martinez, J.C.; Pascoal-Faria, P.; Mateus, A.; Mitchell, G.R. (2022a) In Situ Time-Resolving Small-Angle X-ray Scattering Study of the Injection Moulding of Isotactic Polypropylene Parts. *Mater. Proc. 8*, 30. https://doi.org/10.3390/materproc2022008030
[31] Costa, A.; Gameiro, F.; Potencio, A.; Silva, D.; Carreira, P.; Martinez, J.C.; Pascoal-Faria, P.; Mateus, A.; Mitchell, G.R. (2022b) Evaluating the Injection Moulding of Plastic Parts using In Situ Time-Resolved Small-Angle X-Ray Scattering Techniques Polymers submitted
[32] Liao,T., Zhao, X., Yang, X., Coates, P., Whiteside, B., Barker, D., Thompson G.,, Lai, Y., Jiang, Z., Men, Y., (2021) ”In situ synchrotron small angle X-ray scattering investigation of structural formation of polyethylene upon micro-injection molding” Polymer, **2021**, 215, 123390, doi.org/10.1016/j.polymer.2021.123390.
[33] Zhao,Z., Liao, T., Yang, X., Coates,P., Whiteside, B., Barker,D., Thompson, G., Jiang, Z., Men, Y., (2022) “Mold temperature- and molar mass-dependent structural formation in micro-injection molding of isotactic polypropylene”, Polymer, 248, 124797, doi.org/10.1016/j.polymer.2022.124797.

Commented [M1]: Please carefully check the accuracy of names and affiliations.

[34] Okesola BO, Vieira VM, Cornwell DJ, Whitelaw NK, Smith DK. (2015) 1,3:2,4-Dibenzylidene-D-sorbitol (DBS) and its derivatives--efficient, versatile and industrially-relevant low-molecular-weight gelators with over 100 years of history and a bright future. Soft Matter. 2015 Jun 28;11(24):4768-87. doi: 10.1039/c5sm00845j.

[35] Balkaev, D., Neklyudov, V., Starshinova, V., Stolov, M., Amirova, L.M., Ziyatdinov A., Amirov, R.R., (2021) "Novel nucleating agents for polypropylene and modifier of its physical-mechanical properties", Materials Today Communications, 2021, 101783 doi.org/10.1016/j.mtcomm.2020.101783.

[36[A.Nogales, R.H.Olley and G.R.Mitchell 2003a Directed Crystallisation of Synthetic Polymers by Low-Molar-Mass Self-Assembled Templates *Macromolecular Rapid Comm.* 24 496-502 2003

[37] A.Nogales, G.R. Mitchell, A.S.Vaughan 2003b Anisotropic crystallization in polypropylene induced by deformation of a nucleating agent network Macromolecules 36 4898-4906 2003

[38] Mitchell GR, Pratumshat S, Olley R. (2019) Polyethylene and the Nucleating Agent: Dibenzylidene Sorbitol, a Neutron Scattering Study. AMM 2019;890:199–204. https://doi.org/10.4028/www.scientific.net/amm.890.199.

[39] Wypych, G., and Wypych, A., 2016 "Databook of Nucleating Agents" Elsevier eBook ISBN: 9781927885130

[40] Wangsoub S, Davis FJ, Mitchell GR, et al. (2008) Enhanced Templating in the Crystallization of Poly (ε-caprolactone) using 1,3:2,4-di(4-chlorobenzylidene) sorbitol Macro mol Rapid Commune 29: 1861–1865..

[41] Wangsoub, S., and Mitchell, G.R. Shear controlled crystal size definition in a low molar mass compound using a polymeric solvent Soft Matter, 2009, 5, 525

[42] Mitchell GR, Olley RH. Orthogonal Templating Control of the Crystallisation of Poly(ε-Caprolactone). Polymers (Basel). 2018 Mar 11;10(3):300. doi: 10.3390/polym10030300.

[43] Fernández-García, Marta, Avalos-Belmontes, Felipe, Ramos-deValle, Luis Franc isco, Espinoza-Martínez, Adriana Berenice, Martínez-Colunga, Juan Guillermo, Ramírez-Vargas, Eduardo, Sánchez-Valdés, Saul, Ortíz-Cisneros, Jose Carlos, Martínez-Segovia, Esperanza Elizabeth Beltrán-Ramírez, Flora Itzel (2016) "Effect of Different Nucleating Agents on the Crystallization of Ziegler-Natta Isotactic Polypropylene" - International Journal of Polymer Science 687-9422 doi.org/10.1155/2016/9839201

[44] Ana Tojeira and G.R.Mitchell "Controlling Morphology in 3-D Printing" in "Controlling Controlling the Morphology of Polymers: Multiple Scales of Structure and Processing." Springer 2016 ISBN 978-3-319-39320-9 eds Geoffrey Mitchell and Ana Tojeira

[45] Gibson, Ian, Rosen, David, Stucker, Brent Additive Manufacturing Technologies 3D Printing, Rapid Prototyping, and Direct Digital Manufacturing 2015 Springer ISBN 978-1-4939-2113-3,

[46] da Silva D.P., Pinheiro, J., Abdulghani, S., Kamma-Lorger, C., Martinez, J.C., Solano, E., Mateus, A., Pascoal-Faria, P., and Mitchell, G.R., (2022b) "Property mapping of LDPE during 3D printing: A study on morphological development" Polymers in press

[47] Costa, A.A., Gameiro, F., Potêncio, A., da Silva D.P.,, Carreira, P., Martinez, J.C., Pascoal-Faria, P., Mateus, A., and Mitchell, G.R., (2022b) "Evaluating the Injection Moulding of Plastic Parts using In Situ Time-Resolved Small-Angle X-Ray Scattering Techniques" Polymers in press